Colour Images from
Compound Semiconductor Radiation Detectors
Chapter 3

Alan Owens

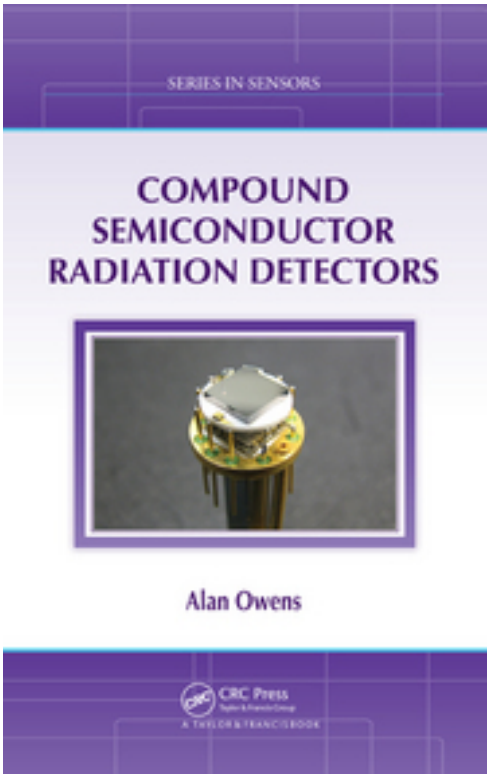

Figure 3.2: Left: a diamond disk saw. Right: a wire saw used for cutting ingots into slices prior to detector preparation. (Images; courtesy European Space Agency and Kromek®).

Figure 3.4: Etching cabinet with automatic titration system for preparing different etch solutions. The cabinet also contains services such as a de-ionized water supply and compressed air system to clean and dry the crystals (Image; courtesy European Space Agency).

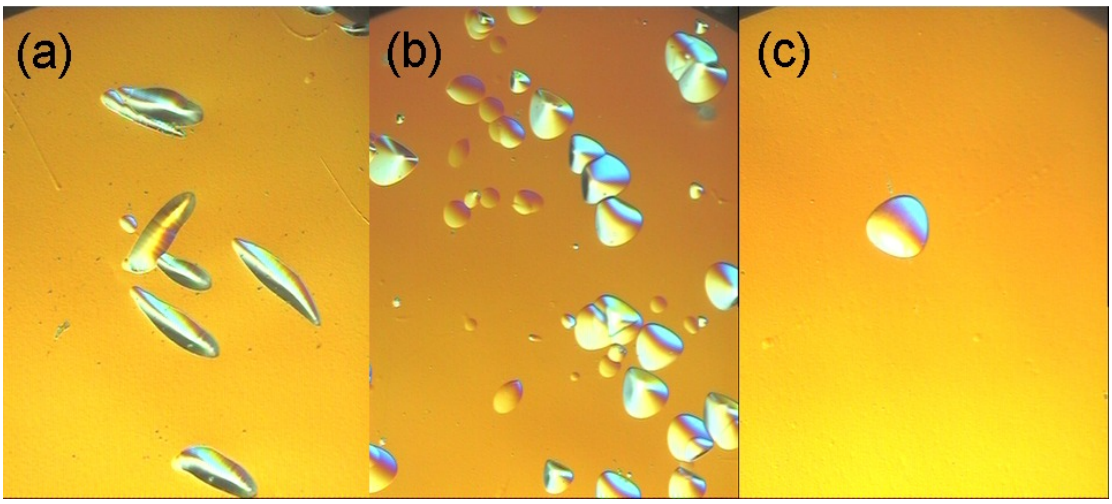

Figure 3.5: Dislocation etch pits in Si, showing the effects of preferential etching along different crystallographic directions. In the [100] orientation, the etch pits appear elliptical in shape whereas along the [111] direction they can assume triangular or pyramidal shapes: b) and c).

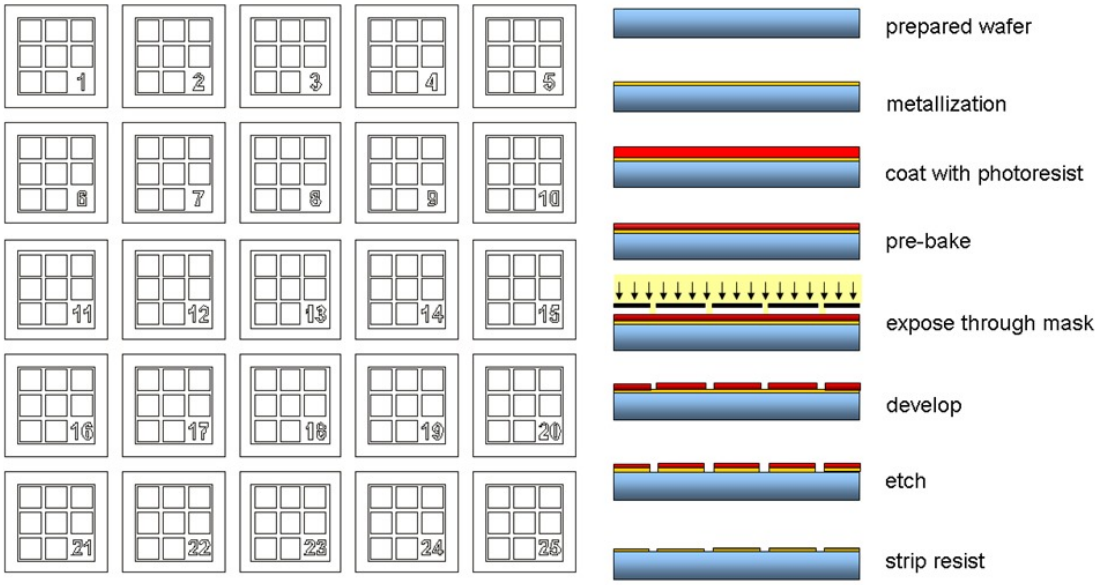

Figure 3.6: Left: a photolithographic mask used to produce a number of 3×3 InAs pixel arrays with guard rings (Image courtesy Oxford Instruments Analytical Oy). Right: example of a typical sequence of lithographic processing steps for forming the contacts to an array, illustrated for a positive resist.

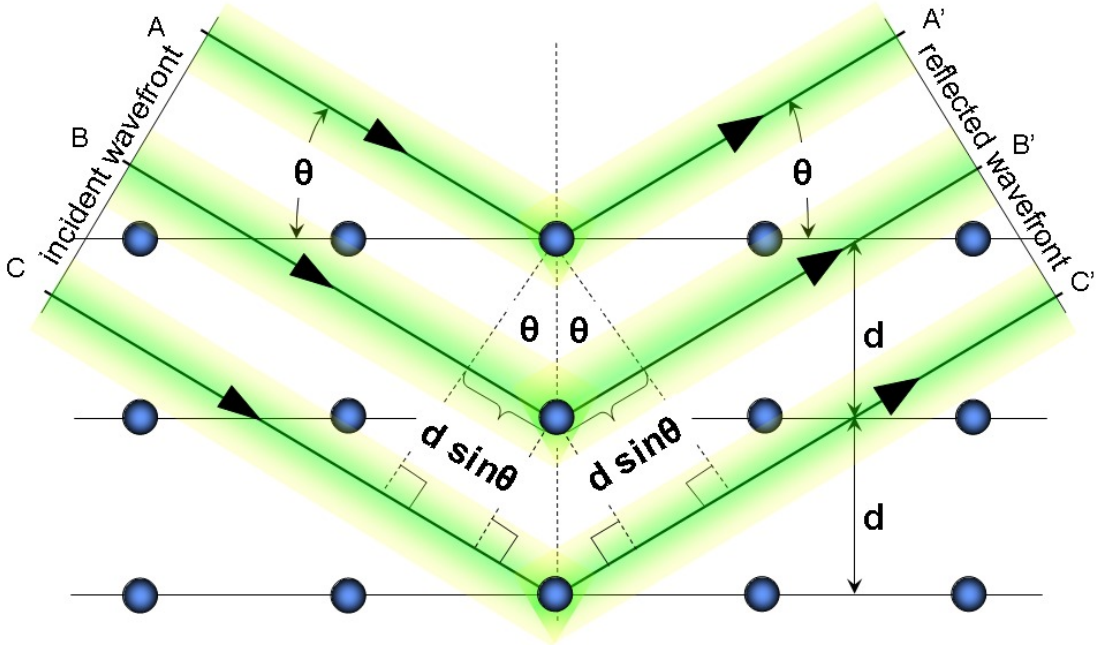

Figure 3.7: Schematic illustrating Bragg reflection. The diffracted x-rays exhibit constructive interference when the distances between paths AA' and BB' and CC' differ by integer numbers of wavelengths (λ).

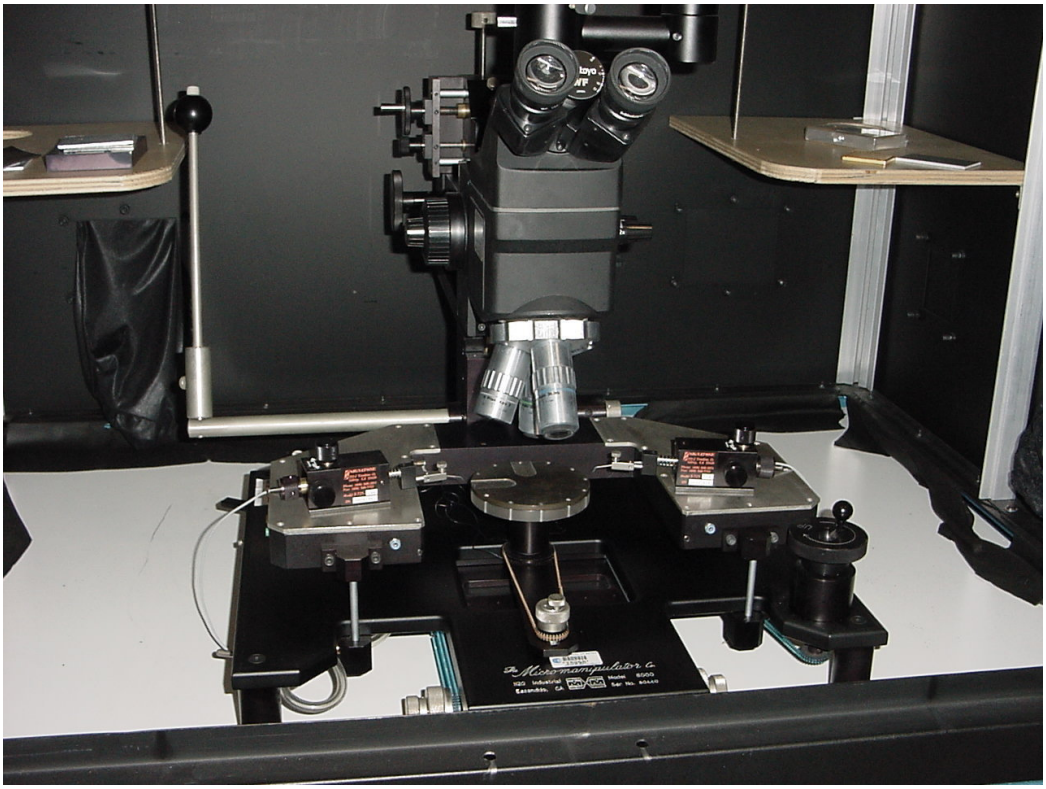

Figure 3.11: A Micromanipulator 6000 series Probe Station. The sample is held on the central 4 inch diameter chuck by vacuum suction. It can be raised to contact the micro-manipulator needles (2 shown) with a positional accuracy of a few microns using the microscope. The chuck can also rotate through 360° and can move ±2 inches in X and Y and ±0.7 inches in Z (the vertical direction).

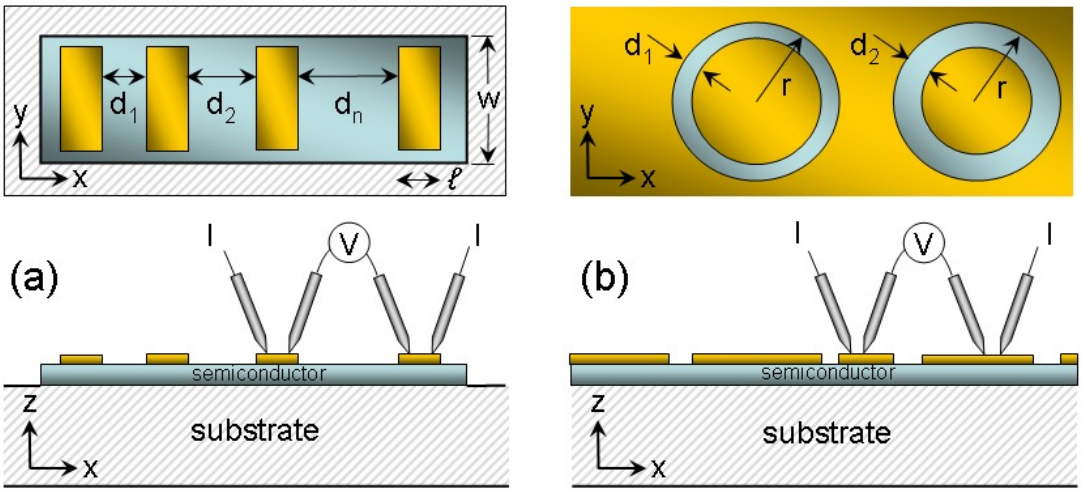

Figure 3.14: Contact resistance test patterns (from [12]), (a) measurement configurations for the transfer length method (TLM) and (b) circular transfer length method (CTLM). For the TLM measurement, the semi-conductor has been etched away around the contacts to form a mesa in order to restrict current flow to adjacent contacts. For both TLM and CTLM, measurements are usually carried out using a four probe technique as illustrated in the cross-sectional views.

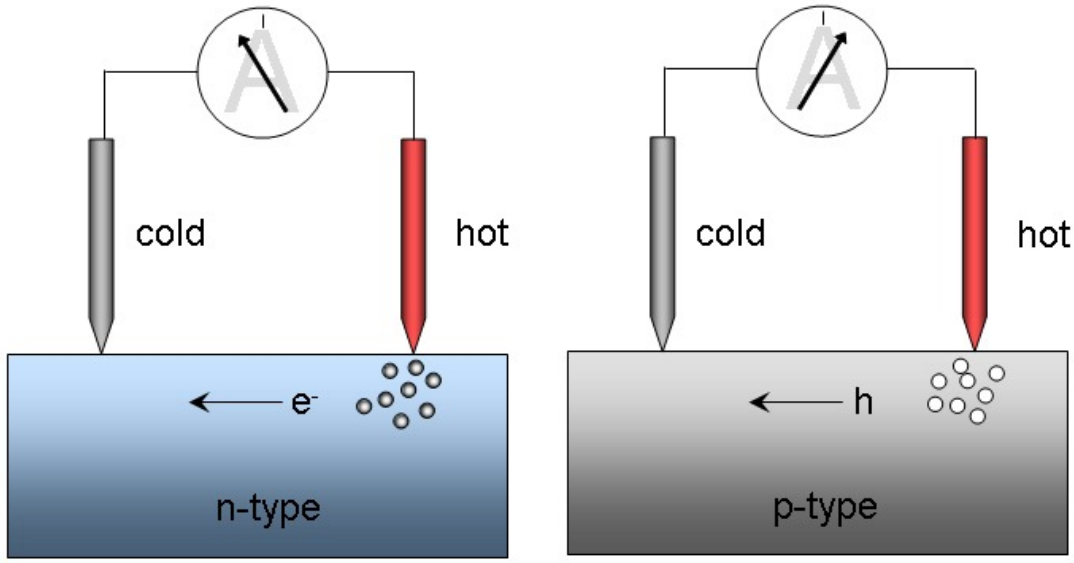

Figure 3.17: Illustration of the hot probe technique for determining the majority carrier type in semiconductors. Carriers diffuse more rapidly near the hot probe. This leads a flow of majority carriers away from the hot probe and a resultant electrical current towards (p-type) or away from (n-type) the hot probe.

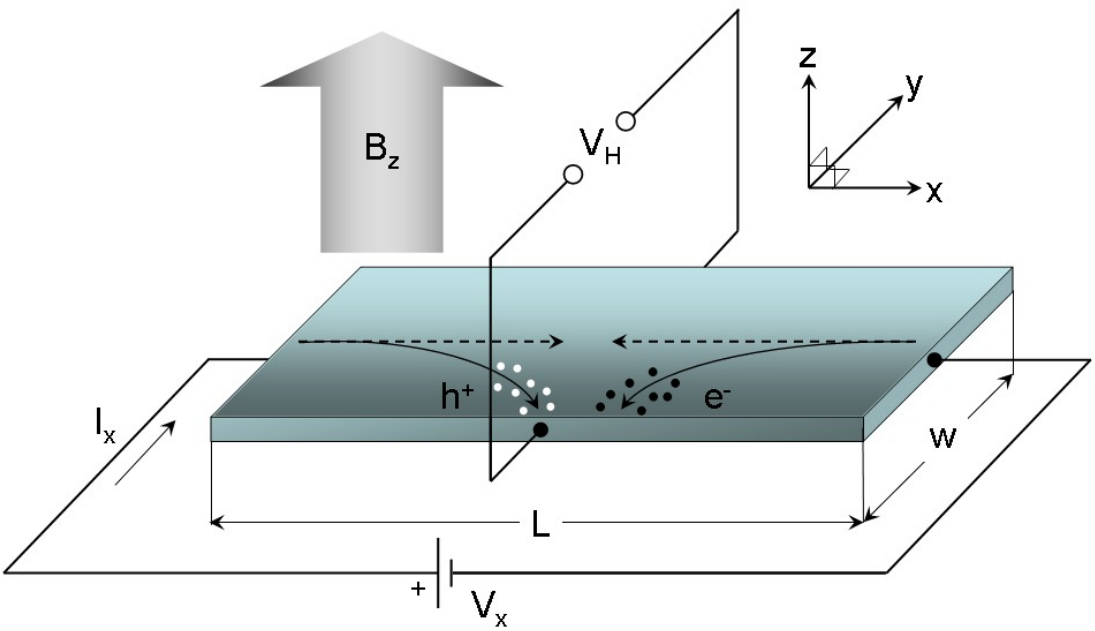

Figure 3.18: Schematic illustrating the sign convention and terminology for the Hall effect.

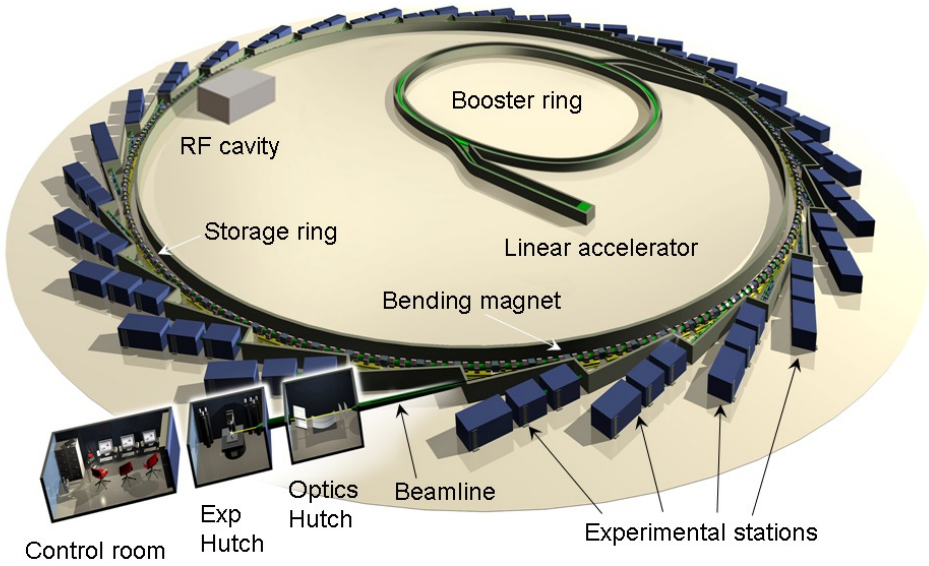

Figure 3.27: Schematic of the third-generation 3 GeV Diamond Light Source [47] at Harwell, Oxford, UK showing its major components. The ring is not truly circular, but is shaped as a twenty-four-sided polygon with a beamline at each vertex. Each beamline is optimised to support an experimental station which specializes in a specific area of science, including the life, physical and environmental sciences. The stations themselves are generally comprised of an optics hutch, experimental hutch and a control room. (Image courtesy Diamond Light Source 2011).

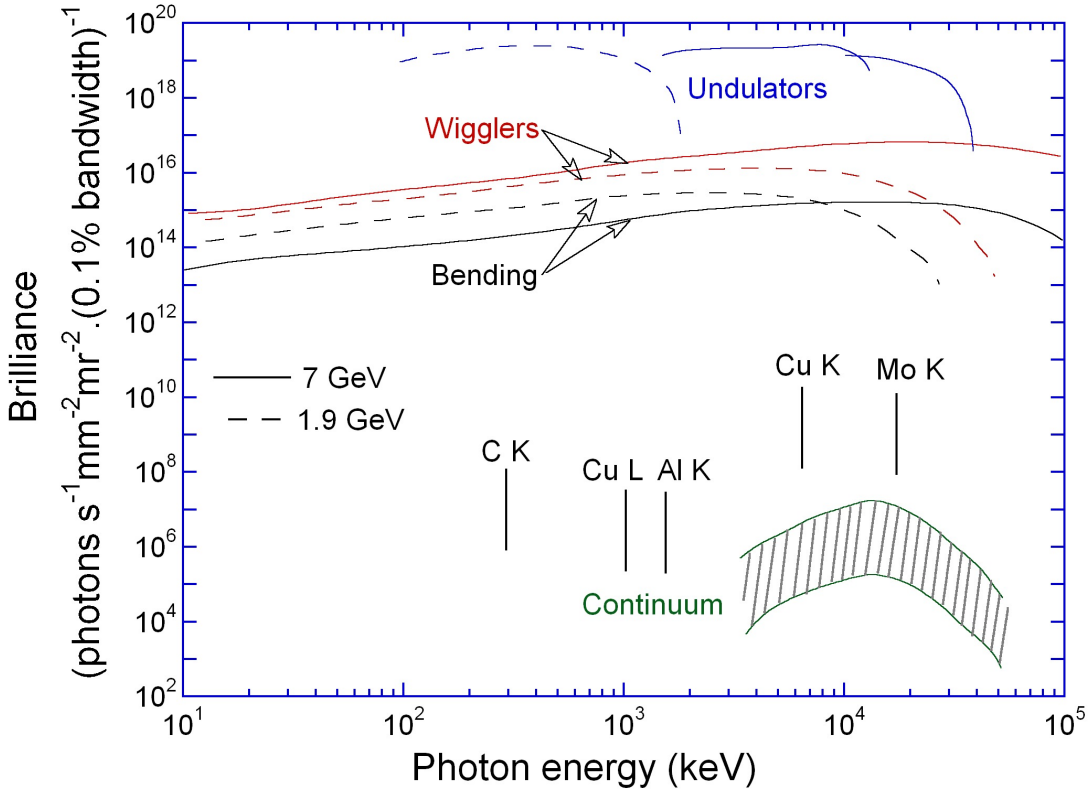

Figure 3.28: Spectral brilliance for several synchrotron radiation sources and conventional X-ray sources. The data for conventional X-ray tubes should be taken as rough estimates only, since brightness strongly depends on operating conditions (adapted from [48], courtesy LBNL).

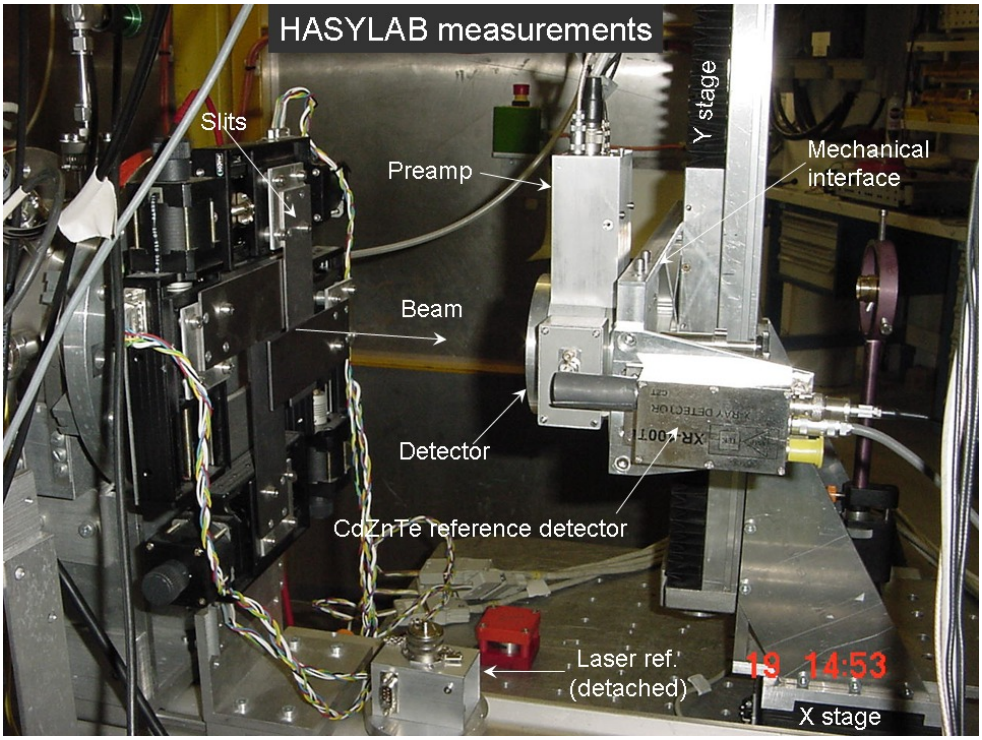

Figure 3.30: Photograph showing the installation of a detector ready for characterization on beamline X1 at the HASYLAB synchrotron research facility at DESY. A laser attached to the front of the detector is used to align its aperture with the center of the slits. A co-aligned reference detector is then used to establish precisely the position of the beam with respect to the detector principle axis prior to scanning.